Available online at www.sciencedirect.com

ScienceDirect

Ceramics International 40 (2014) 4875–4878

CERAMICS INTERNATIONAL

www.elsevier.com/locate/ceramint

Preparation and electrical properties of $Ni_{0.6}Mn_{2.4-x}Sn_xO_4$ NTC ceramics

Zhongbing Wang[a,*], Zhenbo Li[a], Yi Zhang[a], Ruyian Zhang[a], Pan Qin[a], Chunnian Chen[a], Louis Winnubst[b]

[a]School of Chemical Engineering, Anhui Key Laboratory of Controllable Chemistry Reaction & Material Chemical Engineering, Hefei University of Technology, Hefei, Anhui 230009, PR China

[b]Inorganic Membranes, MESA+ Institute for Nanotechnology, University of Twente, P.O. Box 217, 7500 AE Enschede, The Netherlands

Received 5 August 2013; received in revised form 10 September 2013; accepted 10 September 2013
Available online 16 September 2013

Abstract

In this paper spinel-type negative temperature coefficient (NTC) ceramic materials with general composition $Ni_{0.6}Mn_{2.4-x}Sn_xO_4$ ($x=0.1$, 0.2, 0.3, 0.4 and 0.5) were investigated. Powders were prepared by a solid-state reaction method and it was shown that the calcination temperature necessary for formation of the spinel phase as well as the lattice parameter increased with increasing Sn content (x). The specific resistivity at 25 °C and the B value of the ceramics increased sharply by adding more Sn. This increase was correlated with the distribution of the Sn^{4+} ions on the B-sites of the spinel lattice. The materials studied in this work are promising systems for NTC ceramics because of their high resistivity and B values.

Keywords: C. Electrical properties; D. Spinel; NTC; X-ray diffraction

1. Introduction

In recent years negative temperature coefficient (NTC) ceramics have been extensively used for temperature measurement and control in various industrial and domestic applications such as circuit compensation in e.g. aero-space, cryogenic and automotive applications. NTC ceramics are semiconducting materials consisting of 3d transition metal oxides with the spinel structure of the general formula AB_2O_4, based on the oxides of Mn, Ni, Fe, Co, Cu, and Zn etc. In the spinel structure O^{2-} forms a nearly cubic close-packed lattice, where two lattice sites are available for the cations: a tetrahedral (the A-site) and an octahedral site (the B-site) [1–3].

Nickel manganite-based systems are the most widely used NTC thermistors [4]. The electrical properties of these nickel manganites are explained in terms of a phonon assisted hopping of charge carriers between the Mn^{3+} and Mn^{4+} ions as present on octahedral B-sites [5]. In general the electrical properties of these spinel structures strongly depend on composition and microstructure of the ceramic material, because both affect the distribution of the different cations over the A- and B-sites. In order to tune the electrical properties of nickel manganite-based NTC ceramics, much efforts are made on doping this systems with other metals like Co, Fe, Zn, Cr, Cu, Mg, Al, Zr or Si [6–14]. The use of all these additives has greatly broadened the properties and applications of NTC thermistors.

In this paper a new NTC ceramic material, Ni–Mn–Sn–O, was reported. Synthesis conditions and crystal structure of $Ni_{0.6}Mn_{2.4-x}Sn_xO_4$ ($x=0.1$, 0.2, 0.3, 0.4 and 0.5) NTC ceramics were investigated. The distribution of Sn^{4+} ions in the spinel structure was discussed and correlated with the electrical properties.

2. Experimental

High-purity Mn_3O_4, Ni_2O_3, and SnO_2 (AR, Shanghai Chemical Reagent Co. Ltd., China) powders were weighed in appropriate amounts to fabricate $Ni_{0.6}Mn_{2.4-x}Sn_xO_4$ with $x=0.1$, 0.2, 0.3, 0.4 or 0.5. The powder mixture was milled for 6 h in absolute ethanol using a planetary mill and zirconia balls as grinding media. The obtained slurries were dried at 80 °C in an oven for 12 h and

*Corresponding author. Tel.: +86 551 62901451; fax: +86 551 62901450.
E-mail address: zbwang@hfut.edu.cn (Z. Wang).

0272-8842/$ - see front matter
http://dx.doi.org/10.1016/j.ceramint.2013.09.037

subsequently calcined for 6 h at temperatures varying from 950 °C till 1200 °C. The calcined powders were milled again in ethanol, dried, blended with an organic binder (PVA, n=1750, Shanghai Chemical Reagent Co. Ltd., China), sieved (200 mesh), uniaxially pressed at 60 MPa into disks with a diameter of 6 mm and a thickness of 2 mm and finally isostatically pressed at 300 MPa. The green compacts were heated in air to 400 °C at a rate of 100 °C/h and kept at that temperature for 2 h to remove the organic binder, and further heated to 1250 °C at a rate of 250 °C/h and kept at that temperature for 4 h for sintering and finally furnace-cooled to room temperature.

In order to study the crystal structure, sintered samples were crushed and subsequently powder XRD measurements were performed using a PHILIPS X'Pert diffractometer (CuK_α) with a step size of 0.02° and 2θ range from 10° to 70°. Lattice parameters were fitted by the Unitcell software using the least square method. The microstructure of polished and thermally etched as-sintered ceramics was investigated by a scanning electron microscope (SEM; Hitachi S4200). For electrical resistance measurements, the two opposite sides of the sintered disks were polished and coated with silver paste, heated at 850 °C for 15 min for metallization and quenched to room temperature. Silver wires were attached as electrode leads. The electrical resistance was measured in an oil bath at 25 °C and 50 °C by a two-probe technique using an Agilent34401A digital multimeter. The thermal constant B was calculated according to the formula $B=3853.89^{*}\ln(R_{25}/R_{50})$ [7], in which R_{25} and R_{50} are resistances at 25 °C and 50 °C, respectively.

3. Results and discussion

3.1. Phase structure

X-ray diffraction (XRD) is an effective tool to determine the crystal structure, crystallinity and purity of materials. Typical powder XRD patterns of several $Ni_{0.6}Mn_{2.4-x}Sn_xO_4$ materials are given in Fig. 1. The XRD data were analyzed using the PowderX software [15]. $K\alpha_2$ radiation was stripped and the background was subtracted. For x=0.1 ($Ni_{0.6}Mn_{2.3}Sn_{0.1}O_4$), calcined at 950 °C (Fig. 1a), the SnO_2 phase still exists. However, this SnO_2 phase disappears when this system is calcined at 1000 °C, while a single spinel phase is formed. With increasing Sn content a higher calcination temperature is necessary for the formation of a pure, single-phase, spinel structure, e.g. $Ni_{0.6}Mn_{2.1}Sn_{0.3}O_4$ and $Ni_{0.6}Mn_{1.9}Sn_{0.5}O_4$ form a spinel phase after calcination at 1150 °C and 1200 °C respectively (see Fig. 1b and c).

The lattice parameters of the spinel phase for the different compositions, as calculated with the Unitcell software, are presented in Fig. 2. It can be seen that the values increase with increasing Sn content. This is due to the larger radius of Sn^{4+} (0.71 Å, Shannon radius) if compared with Mn^{3+} (0.58 Å). Relative densities (ρ_{rel}) were calculated, using the formula $\rho_{rel}=\rho/\rho_{th}$, where the density ρ of the sintered sample was measured using the Archimedes method and the theoretical density ρ_{th} is calculated from the lattice parameters derived from XRD analysis. After sintering all ceramics have a relative density of more than 95%, indicating that the ceramics were well densified during sintering.

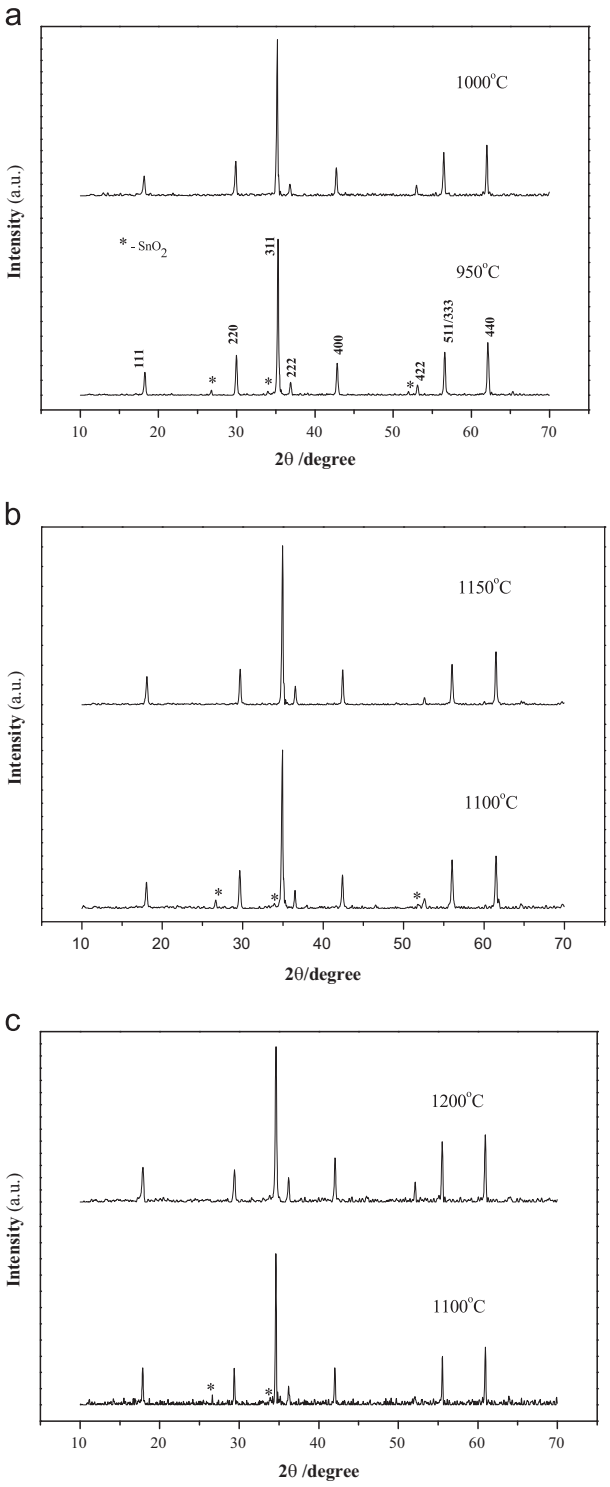

Fig. 1. X-ray diffraction patterns of $Ni_{0.6}Mn_{2.3}Sn_{0.1}O_4$ (Fig. 1a), $Ni_{0.6}Mn_{2.1}Sn_{0.3}O_4$ (Fig. 1b) and $Ni_{0.6}Mn_{1.9}Sn_{0.5}O_4$ (Fig. 1c).

The microstructures of the sintered samples were examined with scanning electron microscopy. A typical SEM image of the as-prepared samples, as given in Fig. 3 shows a dense material with few, closed, pores and a relative uniform grain size in the range 3–10 μm.

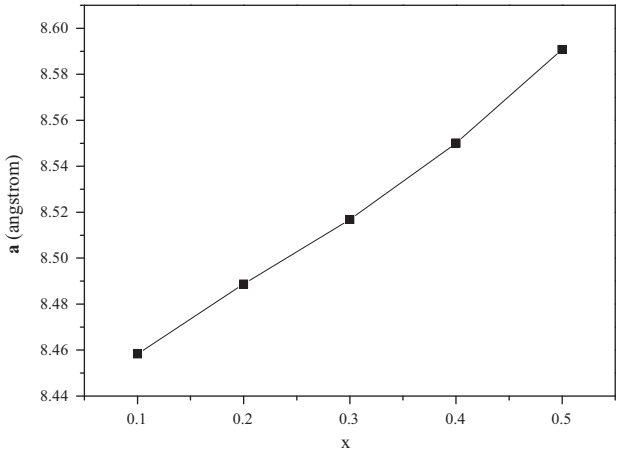

Fig. 2. Lattice parameter for the $Ni_{0.6}Mn_{2.4-x}Sn_xO_4$ series.

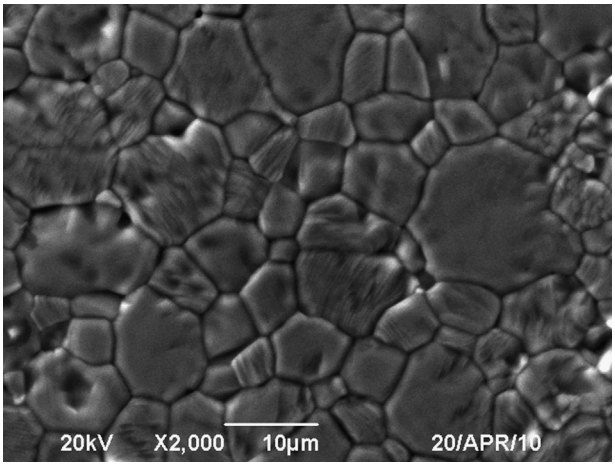

Fig. 3. SEM micrograph of the as-sintered $Ni_{0.6}Mn_{2.1}Sn_{0.3}O_4$ ceramic.

3.2. Distribution of Sn^{4+} ions in the spinel structure

The distribution of the cations in the spinel structure is a subject of many studies, since the physical properties (e.g. magnetic, semiconducting, catalytic, etc.) of these materials are strongly related to the location of the cations in the lattice [16]. Various methods have been used to study the cation distribution, like X-ray diffraction (XRD), neutron diffraction, infrared (IR) spectroscopy and Mössbauer spectroscopy [17–20], of which X-ray diffraction is the most valid and convenient method. In $Ni_{0.6}Mn_{2.4-x}Sn_xO_4$ spinels the Mn^{3+}, Mn^{4+} and Ni^{2+} ions prefer to occupy the B-site, while Mn^{2+} ions tend to reside at the A-site [21]. So only the location of the of Sn^{4+} ions over the A and/or B-site of the spinel structure has to be analyzed by XRD.

It is known that the intensities of the XRD reflections are closely related to the distribution of cations in the spinel lattice and these intensities can be calculated by using the formula as proposed by Buerger [22] $I_{hkl}=|F_{hkl}|^2 \cdot P \cdot L_P T\ A$, where I_{hkl} is the integrated intensity of the XRD signal, F_{hkl} a structural factor, P the multiplicity factor for the plane (hkl) and L_P the Lorentz polarization factor, where $L_P=(1+\cos^2 2\theta)/(\sin^2\theta \cos\theta)$. If one makes use of the intensity ratios of the peaks, the absorption factor (A) and temperature factor (T) do not need to be taken into account, because these constants do not affect the relative intensities for spinels at room temperature. For the $Ni_{0.6}Mn_{2.4-x}Sn_xO_4$ series, having all the same space group, the relative intensity ratio of the reflections is only determined by the structural factor F_{hkl} which in turn is determined by the distribution of the cations over A- or B-sites. By making use of the Powdercell software one can examine in which way the intensity ratio of the reflections is affected by the cation distribution in the AB_2O_4 spinel [23]. From simulation calculations, by using this Powdercell software, it can be concluded that, if more heavy ions occupy the A-site, the relative intensity of the (220) reflection increases, whereas the relative intensity of the (222) and (400) reflections decreases, while, on the other hand the relative intensity of the (220) reflection decreases with a simultaneous increase in relative intensity of the (222) and (400) reflections, if more heavy ions occupy the B-site of the spinel lattice. The relative XRD intensities of the (220), (222) and (400) reflections of the $Ni_{0.6}Mn_{2.4-x}Sn_xO_4$ series are listed in Table 1. Clearly the relative intensity of (220) reflection show a reduced trend, while the relative intensity of the (222) and (400) reflections increase with increasing tin content, x, indicating that the Sn^{4+} ions preferentially occupy the B-sites.

3.3. Electrical properties

Fig. 4 shows the specific resistivity at 25 °C and B values of the $Ni_{0.6}Mn_{2.4-x}Sn_xO_4$ series. As can be seen from this figure the resistivity and B values increase sharply with increasing Sn content from $x=0.1$ to $x=0.5$. For example, the resistivity at 25 °C and B values of $Ni_{0.6}Mn_{2.3}Sn_{0.1}O_4$ are 5920 Ω cm and 3993 K respectively, while for $Ni_{0.6}Mn_{2.0}Sn_{04}O_4$, the resistivity and B values are 200, 526 Ω cm and 4639 K. It is known that the electrical conductivity of these spinels is via a hopping of electrons between the Mn^{3+} and Mn^{4+} ions as present at the octahedral (B) sites of the spinel lattice [24]. An increase in resistivity and B value occurs when the Sn^{4+} ions preferentially occupy the B-site, because in that case these ions obstruct the route for electron hopping and also lead to a decrease in $[Mn^{3+}]$ and $[Mn^{4+}]$ on the B-sites. In other words, the persistent increase in resistivity of $Ni_{0.6}Mn_{2.4-x}Sn_xO_4$ with increasing Sn content indicates that the Sn^{4+} ions preferentially occupy the B-site, which is in accordance with the results derived from X-ray diffraction. It is noteworthy to mention that the usual method to try to achieve high resistivity and B values in NTC ceramics is by introducing Al into the spinel structure [25]. In this paper we present Sn as an alternative element.

4. Conclusions

In summary, $Ni_{0.6}Mn_{2.4-x}Sn_xO_4$ ($x=0.1$, 0.2, 0.3, 0.4 and 0.5) spinel ceramic powders were synthesized using a solid state reaction. The calcination temperature, necessary for the formation of a pure single spinel phase as well as the lattice parameter increases with increasing of Sn content. These spinels can be sintered into dense ceramics at a temperature of 1250 °C. The specific resistivity at 25 °C and the B values of the ceramics sharply increase by adding more Sn content. This effect is

Table 1
Relative intensities of (220), (222) and (400) XRD reflections for the $Ni_{0.6}Mn_{2.4-x}Sn_xO_4$ series.

	$x=0.1$	$x=0.2$	$x=0.3$	$x=0.4$	$x=0.5$
I_{220}	21.98	21.82	21.53	20.26	20.02
I_{222}	7.32	8.39	11.60	12.02	15.71
I_{400}	17.83	19.13	21.95	24.14	28.62

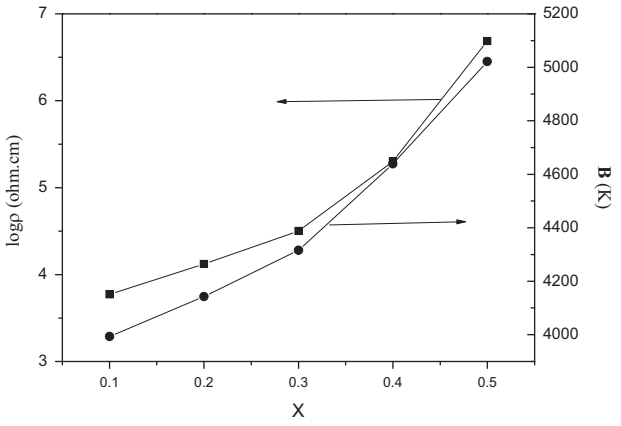

Fig. 4. Specific resistivity at 25 °C and B values for the $Ni_{0.6}Mn_{2.4-x}Sn_xO_4$ series as a function of Sn content, x.

correlated with the distribution of the Sn^{4+} ions over the B-sites of the spinel lattic. These $Ni_{0.6}Mn_{2.4-x}Sn_xO_4$ ceramics are new promising materials for NTC ceramics with high resistivity and B values.

Acknowledgment

This work was financially supported by the Anhui Provincial Natural Science Foundation (Grant no. 1208085ME85).

References

[1] A. Rousset, R. Legros, A. Lagrange, Recent progress in the fabrication of ceramic negative temperature coefficient thermistors, Journal of the European Ceramic Society 13 (1994) 185–189.
[2] Kurt E. Sickafus, John M. Wills, Norman W. Grimes, Structure of spinel, Journal of the American Ceramic Society 82 (1999) 3279–3292.
[3] F. Antonia, Negative temperature coefficient resistance (NTCR) ceramic thermistors: an industrial perspective, Journal of the American Ceramic Society 92 (2009) 967–983.
[4] Daolai Fang, Zhongbing Wang, Pinghua Yang, Wei Liu, Chusheng Chen, Preparation of ultra-fine nickel manganite powders and ceramics by a solid-state coordination reaction, Journal of the American Ceramic Society 89 (2006) 230–235.
[5] E.D. Macklen, Electrical conductivity and cation distribution in nickel manganite, Journal of Physics and Chemistry of Solids 47 (1986) 1073–1079.
[6] T. Yokoyama, T. Meguro, Y. Shimada, J. Tatami, K. Komeya, Y. Abe, Preparation and electrical properties of sintered oxides composed of $Mn_{1.5}Co_{(0.25+x)}Ni_{(1.25-x)}O_4$ ($0 \le x \le 0.75$) with a cubic spinel structure, Journal of Materials Science 42 (2007) 5860–5866.
[7] Zhongbing Wang, Chunhua Zhao, Pinghua Yang, A.J.A. Winnubst, Chusheng Chen, X-ray Diffraction and infrared spectra studies of $Fe_xMn_{2.34-x}Ni_{0.66}O_4$ ($0 < x < 1$) NTC Ceramics, Journal of the European Ceramic Society 26 (2006) 2833–2837.
[8] J. Takahashi, A. Miura, H. Itoh, K. Sawayama, T. Akazawa, K. Nebuka, H. Miura, M. Kishi, Phase change and electrical resistivity of Zn–Mn–Ni–O-based NTC thermistors produced using IZC powder recycled from used dry batteries, Ceramics International 34 (2008) 853–857.
[9] K. Park, I.H. Han, Effect of Cr_2O_3 addition on the microstructure and electrical properties of Mn–Ni–Co oxides NTC thermistors, Journal of Electroceramics 17 (2006) 1069–1073.
[10] Rupali Jadhav, Deepti Kulkarni, Vijaya Puri, Structural and electrical properties of fritless $Ni_{(1-x)}Cu_xMn_2O_4$ ($0 \le x \le 1$) thick film NTC ceramic, Journal of Materials Science: Materials in Electronics 21 (2010) 503–508.
[11] Jiangying Wang, Jingji Zhang, Structural and electrical properties of $NiMg_xMn_{2-x}O_4$ NTC thermistors prepared by using sol–gel derived powders, Materials Science Engineering B 176 (2011) 616–619.
[12] K. Park, I.H. Han, Effect of Al_2O_3 addition on the microstructure and electrical properties of $(Mn_{0.37}Ni_{0.3}Co_{0.33-x}Al_x)O_4$ ($0 \le x \le 0.03$) NTC thermistors, Materials Science Engineering B 119 (2005) 55–60.
[13] K. Park, Microstructure and electrical properties of $Ni_{1.0}Mn_{2-x}Zr_xO_4$ ($0 \le x \le 1$) negative temperature coefficient thermistors, Materials Science Engineering B 104 (2003) 9–14.
[14] K. Park, S.J. Yun, Effect of SiO_2 addition on the electrical stability of $(Mn_{2.1-x}Ni_{0.9}Si_x)O_4$ ($0 \le x \le 0.18$) negative temperature coefficient thermistors, Materials Letters 58 (2004) 933–937.
[15] Cheng Dong, PowderX software, Institute of Physics, Chinese Academy of Sciences.
[16] M.A. Willard, Y. Nakamura, D.E. Laughlin, M.E. McHenry, Magnetic properties of ordered and disordered spinel-phase ferrimagnets, Journal of the American Ceramic Society 82 (1999) 3342–3346.
[17] P.K. Baltzer, J.G. White, Crystallographic and magnetic studies of the system $(NiFe_2O_4)_{1-x}+(NiMn_2O_4)_x$, Journal of Applied Physics 29 (1958) 445–447.
[18] J.M. Hastings, L.M. Corliss, Neutron diffraction study of manganese ferrite, Physical Review 104 (1961) 328–331.
[19] R.D. Waldron, Infrared spectrum of ferrites, Physical Review 99 (1955) 1727–1735.
[20] T. Battault, R. Legros, A. Rousset, Structure and electrical properties of iron manganite spinels in relation with cationic distribution, Journal of the European Ceramic Society 15 (1995) 1141–1147.
[21] W.A. Groen, C. Metzmacher, P. Huppertz, S. Schuurman, Aging of NTC ceramics in the system Mn–Ni–Fe–O, Journal of Electroceramics 7 (2001) 77–87.
[22] M.J. Buerger, Crystal Structure Analysis, Wiley, New York, 1960.
[23] W. Kraus, G. Nolze, Powdercell2.4, Federal Institute for Materials Research and Testing Rudower Chaussee 5, 12489 Berlin, Germany.
[24] S. Fritsch, J. Sarrias, M. Brieu, J.J. Couderc, J.L. Baudour, E. Snoeck, A. Rousset, Correlation between the structure, the microstructure and the electrical properties of nickel manganite negative temperature coefficient (NTC) thermistors, Solid State Ionics 109 (1998) 229–237.
[25] Wang Zhongbing, Wu Lei, Zhao Suying, Han Xiaozhao, Effect of dosage on Ni–Mn–O doped NTC thermo-sensitive ceramics and their electrical properties, Journal of the Chinese Ceramic Society 37 (2009) 927–931.